applied sciences

MDPI

Article

Aluminum Phosphate Nanoplates Synthesized via Green Method Using Cork Oak Somatic Embryo-Derived Phytates

Beatriz Pintos * and Arancha Gomez-Garay

Genetic, Physiology and Microbiology Department, Facultad de Ciencias Biológicas, Universidad Complutense de Madrid, C/José Antonio Novais 12, 28040 Madrid, Spain; magom02@ucm.es

* Correspondence: bpintos@ucm.es

Featured Application: This study on aluminum phosphate nanoparticles ($AlPO_4$NPs) synthesized through green methods has significant implications for advancing nanomaterial synthesis with sustainable practices. By utilizing phytates extracted from *Quercus suber* somatic embryos, the green synthesis approach not only provides a natural precursor for nanoparticle formation but also emphasizes the environmental benefits of using plant-derived materials. The synthesized aluminum phosphate nanoplates, characterized by their unique optical and structural properties, show promising potential applications. This research paves the way for further innovations in nanotechnology and environmental biotechnology, highlighting the role of sustainable methods in the production of high-value nanomaterials.

Abstract: This study presents a novel green synthesis method for aluminum phosphate ($AlPO_4$) nanoplates using extracts from *Quercus suber* somatic embryos. Traditionally, metallic nanoparticles are synthesized using harmful chemical reagents and solvents, but our approach leverages bioactive compounds, such as phytic acid (IP6) from plant extracts, offering a more sustainable alternative. We observed a high phosphate content of 23.6 µMol PO_4^{3-}/mg dry weight (DW) in the extracts, which is significantly higher than in other *Quercus* species. Characterization through UV–VIS spectroscopy and XRD confirmed the formation of complex crystal nanoplates, where anisotropic aluminum phosphate with a triclinic crystal structure coexists with monoclinic structures, both forms of aluminum phosphate tridymite. Electron microscopy (TEM and SEM) revealed the hierarchical organization of these nanoplates, distinguishing them from the more commonly observed spherical nanoparticles. Fourier-transform infrared (FTIR) spectroscopy further validated the incorporation of phytic acid into the nanoplate structure. This innovative method not only advances sustainable nanomaterial synthesis but also demonstrates the potential for unique optical and structural properties in aluminum phosphate nanoplates, paving the way for future applications in specialized fields.

Keywords: green synthesis; aluminum phosphate nanoplates; sustainable methods; natural reducing agents

Citation: Pintos, B.; Gomez-Garay, A. Aluminum Phosphate Nanoplates Synthesized via Green Method Using Cork Oak Somatic Embryo-Derived Phytates. *Appl. Sci.* **2024**, *14*, 8681. https://doi.org/10.3390/app14198681

Academic Editors: Gang Wei and Marco Rossi

Received: 8 August 2024
Revised: 23 September 2024
Accepted: 23 September 2024
Published: 26 September 2024

1. Introduction

Aluminum nanoparticles have garnered significant attention and application across a spectrum of technological and medical domains owing to their distinct physical and chemical properties. In technological applications, these nanoparticles are particularly prized for their ability to enhance the mechanical properties of materials [1]. They are crucial components in the fabrication of high-strength composite materials used extensively in industries demanding lightweight yet durable solutions, such as the aerospace and automotive sectors [2]. The high surface area-to-volume ratio of aluminum nanoparticles also makes them ideal for improving the performance of energy storage devices [3]. By incorporating these nanoparticles into batteries and capacitors, manufacturers can achieve enhanced energy storage capacity, faster charging rates, and improved overall efficiency in

energy storage technologies. Moreover, in the realm of advanced electronics, aluminum nanoparticles contribute to the development of cutting-edge electronic components [4]. Their excellent conductivity and compatibility with semiconductor materials make them invaluable for creating miniaturized devices, high-performance circuits, and other electronic applications where precision and efficiency are paramount.

In the medical field, aluminum nanoparticles exhibit remarkable potential as therapeutic and diagnostic agents [5]. Engineered to be biocompatible and safe for biological systems, these nanoparticles play a pivotal role in targeted drug-delivery systems [6,7]. By functionalizing aluminum nanoparticles with drugs or therapeutic molecules, researchers can precisely deliver treatments to specific tissues or cells within the body. This targeted approach not only enhances treatment efficacy but also minimizes side effects associated with traditional drug-delivery methods. Furthermore, aluminum nanoparticles are integral to emerging therapies such as photothermal therapy [8]. When exposed to certain wavelengths of light, aluminum nanoparticles efficiently convert light energy into heat, enabling precise and localized heating of targeted tissues. This capability is harnessed in cancer treatment to selectively destroy tumor cells while sparing healthy surrounding tissue from damage.

Additionally, aluminum nanoparticles serve as effective contrast agents in medical imaging techniques like MRI (Magnetic Resonance Imaging) and CT (Computed Tomography) scans [9]. Their ability to enhance the visibility of tissues and organs in imaging procedures allows for more accurate diagnosis and monitoring of various medical conditions. By improving the contrast and resolution of imaging, these nanoparticles facilitate the early detection of diseases.

Aluminum phosphate nanoparticles exhibit unique properties that make them valuable in both technological and biomedical applications. In technological contexts, aluminum phosphate nanoparticles are utilized as flame retardants [10,11] and in the production of ceramics and glass [12,13]. Their ability to enhance fire resistance and mechanical strength makes them essential in the construction industry, where safety and durability are critical considerations.

However, traditional methods of synthesizing aluminum nanoparticles present several significant challenges. These conventional methods typically involve complex and energy-intensive chemical processes, such as chemical vapor deposition, sol–gel processes, and ball milling [1]. Such processes often require high temperatures and the use of hazardous chemicals, leading to the generation of substantial amounts of toxic waste. This not only poses serious environmental hazards but also necessitates stringent waste management practices, further increasing the overall operational costs. Moreover, the high energy consumption associated with these traditional synthesis methods contributes to their environmental footprint, making them less sustainable. The substantial energy and material costs involved in these procedures significantly elevate the overall production expenses. As a result, these high costs limit the feasibility of large-scale production of aluminum nanoparticles [14], making it challenging to meet the growing demand in various industrial sectors. Additionally, the high costs hinder the adoption of these technologies in emerging markets, where economic constraints are more pronounced and sustainable, and cost-effective solutions are in greater demand.

In this context, green synthesis emerges as a promising alternative to the production of aluminum nanoparticles. This approach relies on the use of environmentally friendly reagents and reaction conditions, thereby minimizing the generation of toxic waste and energy consumption. The benefits of green synthesis extend beyond reducing environmental impact; they also include cost reduction and improved biocompatibility of the resulting nanoparticles. Therefore, the implementation of green synthesis techniques represents a significant advancement toward the sustainable and economical production of aluminum nanoparticles, opening new opportunities for their application across various industries [15].

The principle behind green synthesis lies in harnessing the reducing power of biomolecules such as phenols, flavonoids, terpenoids, and enzymes present in these natural sources. These biomolecules act as both reducing agents, facilitating the reduction in metal ions (e.g., silver, gold, iron) to their respective zero-valent states, and as stabilizing agents, preventing aggregation and ensuring the stability of the resulting nanoparticles [16]. The process usually involves mixing a precursor solution of metal salts with an extract or biomass under controlled conditions. As the reduction reaction proceeds, nanoparticles nucleate and grow, guided by the biomolecules present in the natural extract.

Phytates, also known as phytic acid or inositol hexaphosphate (IP6), are chemical compounds belonging to the family of polyphosphates. They consist of an inositol ring with six phosphate groups attached at specific positions (Figure 1). Due to their structure, phytates possess the unique ability to form insoluble complexes with metals.

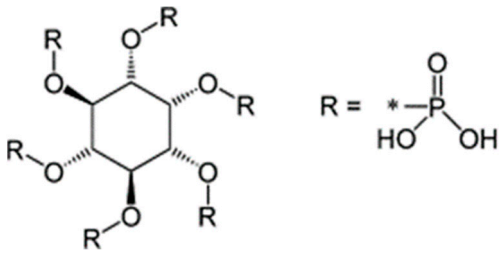

Figure 1. Chemical structure of phytic acid [17].

In green synthesis processes, the presence of phytates (or phytic acid) in plant extracts can play a significant role. Phytates, abundant in various plant tissues [18], act as natural chelating agents due to their ability to bind metal ions through their multiple phosphate groups [19]. In the context of green nanoparticle synthesis, phytates can serve dual roles: they can act as reducing agents, facilitating the reduction in metal ions to form nanoparticles, and as stabilizing agents, preventing the agglomeration of nanoparticles by binding to their surfaces and providing stability.

Phytates serve as phosphorus storage compounds in seeds and grains, playing a crucial role in phosphorus metabolism regulation in plants [20]. In the context of somatic embryos, phytates are notably present due to their analogous role to seeds in mature plants [21]. Somatic embryos are multicellular structures developed in vitro from plant tissues, essentially functioning as initial "seeds" for the growth of new plants. Within these structures, phytates act as natural phosphorus reservoirs, crucial for the metabolism and early growth stages of plants during their initial developmental phase. The presence of phytates in somatic embryos not only ensures the availability of phosphorus essential for early growth but also influences key biological and biochemical processes that support the viability and development of these precursor plant structures.

The objective of this study is to investigate and demonstrate the role of phytates extracted from cork oak somatic embryos in the environmentally friendly synthesis of aluminum nanoparticles. By leveraging their natural chelating and reducing properties, this research aims to advance the green synthesis of sustainable and biocompatible materials. Understanding this process is crucial for exploring applications of these materials in nanotechnology and enhancing the efficiency of eco-friendly synthesis methods.

2. Materials and Methods

2.1. Plant Material and Extract Preparation

The plant materials used in this study included somatic embryos of cork oak obtained from in vitro culture [22].

To prepare the plant extracts, the plant material was first frozen at −20 °C and subsequently lyophilized to remove all water content. The resulting lyophilized powder was stored at room temperature. For the extraction process, 100 mg of this lyophilized powder was weighed and combined with 10 mL of distilled water. The mixture was then incubated

in a water bath at 80 °C with constant agitation for 15 min. After incubation, the solution was centrifuged at 5000 rpm for 10 min to separate the supernatant, which is rich in phytochemicals, from the solid residues of the plant powder. Finally, to ensure complete removal of any plant tissue residues, the supernatant was filtered using a sterile 0.2-micron filter. The filtered extract was stored under refrigeration at 4 °C, in the dark, until use. The shelf life of the extract under these conditions was assessed for up to one month, during which time it retained its effectiveness in nanoparticle synthesis with no significant reduction in yield or quality.

2.2. Determination of Phosphate Content

The phosphate content in somatic embryo extract was calculated using the molybdate blue method. In a dilute orthophosphate solution, ammonium molybdate reacts under acidic conditions to form molybdophosphoric acid, a heteropolyacid. When vanadium is present, yellow vanadomolybdophosphoric acid is produced. The intensity of the yellow color correlates with the phosphate concentration. Absorbance was measured at 470 nm.

2.3. Green Synthesis of Metallic Nanoparticles

The synthesis of metallic nanoparticles began with the preparation of a stock solution of aluminum nitrate nonahydrate, $Al(NO_3)_3 \cdot 9H_2O$, at a concentration of 1 M. This solution served as the metallic precursor for the synthesis of aluminum nanoparticles (AlNPs). A concentration of aluminum nitrate nonahydrate 5 mM was used for the synthesis of the nanoparticles, achieved by mixing 2 mL of extract with 12.5 µL of aluminum nitrate nonahydrate (1 M) and 487.5 µL of distilled water. Subsequently, the mixture was placed in an oven at 60 °C and maintained until complete evaporation of the liquid phase.

2.4. Characterization of Nanoparticles

There are several techniques available for characterizing the physicochemical properties of nanoparticles, including analysis of their shape, size, chemical composition, purity, surface area, and crystalline phase. In this study, the following methods were employed: UV–visible spectroscopy, which provided insights into size, shape, and concentration and enabled identification of the compound through surface plasmon resonance (SPR) detection for metallic NPs. X-ray diffraction (XRD) played a crucial role in determining the crystalline system, size, and crystallization orientations in both amorphous and crystalline phases. Transmission electron microscopy (TEM) was employed to examine the microstructures, allowing for detailed observation of NPs size and morphology. Scanning electron microscopy (SEM) provided detailed images of the surface morphology. Energy-dispersive X-ray spectroscopy (EDX) was used in conjunction with TEM and SEM to analyze the elemental composition of the sample. Finally, Fourier-transform infrared spectroscopy (FTIR) was utilized to identify functional groups and assess the chemical composition of the NPs.

2.4.1. UV–Visible Spectroscopic Analysis

A cuvette was prepared with 2.5 mL of the extract and using sterile distilled water as a blank. UV–Vis spectroscopy was also used to measure the absorbance of the plasmon responsible for the characteristic color observed during the synthesis of nanoparticles [23]. This technique was employed because, during nanoparticle synthesis, the color of the plant extract darkened, indicating nanoparticle formation, at which point an absorbance peak was recorded.

This spectroscopic study was conducted over a wavelength range of 200 nm to 700 nm with a UV–Vis (Genesys 10S UV-Vis, Thermo Fisher Scientific, Shanghai, China). Both the extract and the metallic nanoparticles obtained were analyzed at 15-min intervals without agitation until one hour, at which measurements were taken both with and without agitation.

2.4.2. X-ray Powder Diffraction (XRD)

The X-ray powder diffraction (XRD) profiles were obtained using an X Bruker D8 ADVANCE diffractometer, with a 2-theta range from 5 to 90 degrees. The analyses were conducted at the Research Support Centre (CAI) for X-ray Diffraction of the Universidad Complutense de Madrid, Ciudad Universitaria s/n, 28040 Madrid, Spain. The resulting diffraction patterns were compared with reference patterns from the International Centre for Diffraction Data (ICDD) database.

2.4.3. Transmission Electron Microscopy (TEM)

The nanoparticles were dispersed in 1 mL of water. TEM grids were prepared by placing a drop of the nanoparticle solution on a carbon-coated copper grid and allowing it to dry at room temperature. TEM analysis was conducted using a JEOL 2100 microscope at the Centro Nacional de Microscopía Electrónica, Av. Complutense s/n, 28040 Madrid, Spain.

2.4.4. Scanning Electron Microscopy (SEM)

Scanning electron microscopy (SEM) images were recorded on a JEOL 7600 F instrument at the Centro Nacional de Microscopía Electrónica, Av. Complutense s/n, 28040 Madrid, Spain.

2.4.5. Energy-Dispersive X-ray Spectroscopy (EDX)

This technique was used to understand the chemical composition and distribution of elements within the NP sample. The analysis was performed at the Centro Nacional de Microscopía Electrónica, Av. Complutense s/n, 28040 Madrid, Spain.

2.4.6. Fourier-Transform Infrared Spectroscopy (FTIR)

Fourier-transform infrared (FTIR) spectroscopy measurements were performed using a JASCO FT/IR-6200 spectrophotometer at the CAI of Physical and Chemical Techniques, spectroscopy and Correlation Unit, of the Complutense University of Madrid, Plaza de Ciencias, 2, 28040 Madrid, Spain. The results were analyzed and interpreted according to the tables included in Callejas [24].

3. Results

3.1. Phytochemical Yield: Phosphate and Phytate Contents

The extraction process was efficient, yielding clear, phytochemical-rich supernatants from the plant material (somatic embryos of cork oak).

The phosphate content in the extract from cork oak somatic embryos was determined to be 23.6 µMol PO_4^{3-}/mg DW, indicating a relatively high concentration of phosphate. This high level of phosphate is likely due to the presence of phytic acid.

3.2. Synthesis of Metallic Nanoparticles

The formation of aluminum nanoparticles (AlNPs) via green synthesis was visually confirmed by observing the color change in the aqueous extract of cork oak somatic embryos upon the addition of aluminum nitrate nonahydrate (Figure 2). Initially, the mix exhibited a light yellow color, which gradually darkened to a deep yellow–brown over several hours, indicating the progression of the reaction. Concurrently, "white clouds" formed within the extract, slowly settling at the bottom and middle of the container (Figure 2B–D).

This color change became more pronounced when the extracts were incubated with 5 mM aluminum nitrate nonahydrate in an oven at 60 °C for several days. As the water evaporated, the color intensified, becoming progressively darker. After three days, once all the water had evaporated, spherical, crystalline, and porous structures were observed at the bottom corners of the container. These structures represent the final product of the aluminum nitrate nonahydrate reduction by the phytochemicals in the plant extract (Figure 2F).

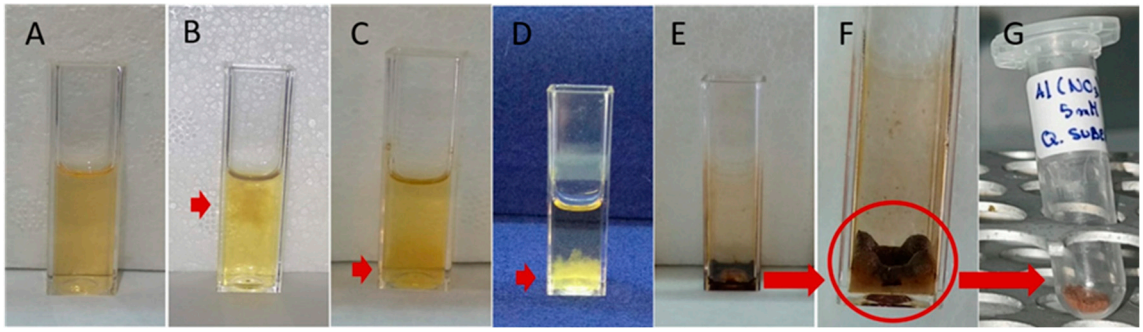

Figure 2. Formation of aluminum nanoparticles from the reaction of the aqueous extract of cork oak embryos obtained in vitro with aluminum nitrate nonahydrate (5 mM). (**A**–**G**) Time-lapse of the synthesis. (**A**) Mixing of the aqueous extract of cork oak embryos obtained in vitro with aluminum nitrate nonahydrate at time = 0. (**B**) Formation of a "cloud" at the top of the beaker. (**C**,**D**) The whitish cloud moves to the bottom of the beaker (the beaker in (**D**) is placed on a blue background for better visualization). (**E**) Dark precipitation at the bottom of the beaker. (**F**) Formation of globular structures in the corners of the beaker after drying and consequent removal of the supernatant. (**G**) Eppendorf tube with the characteristic powder-like material collected from the beaker for further characterization.

3.3. UV–Visible Spectroscopic Analysis

UV–visible spectroscopic analysis was conducted to examine the aluminum phosphate nanoplates synthesized using the cork oak extract. This analysis aimed to investigate the optical properties and confirm the formation of the nanoplates.

The UV–visible spectra revealed a distinct absorption peak, indicative of the aluminum phosphate nanoplates (Figure 3). The observed peak, typically associated with the surface plasmon resonance (SPR) of metallic nanoparticles, confirmed the presence and formation of aluminum phosphate nanoplates. Notably, an absorption peak was observed at 402 nm, corresponding to the long wave region, which is characteristic of these nanoparticles.

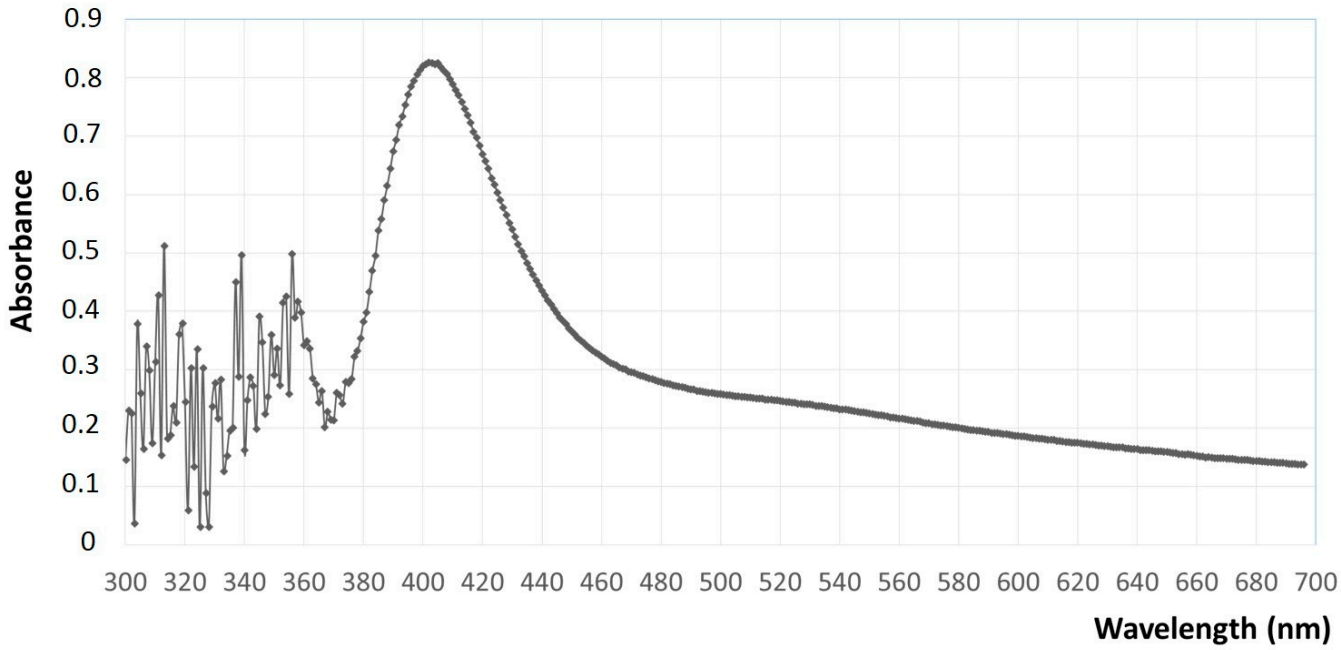

Figure 3. The absorbance spectra from a dispersion of aluminum phosphate nanoparticles obtained by green synthesis from $Al(NO_3)_3 \cdot 9H_2O$ and cork oak somatic embryos extract.

3.4. X-ray Powder Diffraction (XRD)

The XRD patterns of the nanoparticles synthesized using cork oak extract showed distinct peaks corresponding to aluminum phosphate. The prominent peaks at specific 2 theta values matched the reference patterns for aluminum phosphate ($AlPO_4$), confirming its presence (Figure 4).

Intense diffraction peaks were observed at the following 2θ values: 27.32°; 29.74°; 32.74°; 39.31°; and 44.69°. These peaks indicate the presence of aluminum phosphate, corresponding to the reference 04-018-2837 from the ICDD database. Other peaks at 2θ values were 23.51°, 41.54°, and 43.65°, which corresponded to the reference 05-001-0464 from the ICDD database. Thus, the XRD analysis revealed that the synthesized aluminum phosphate nanoplates exhibited two distinct crystal systems. The primary crystal system identified is triclinic (anorthic), as matched with the reference pattern 04-018-2837 from the ICDD database. This system is characterized by its low symmetry, where all three axes have different lengths, and none of the angles are 90°. Such irregularity in the crystal structure is uncommon and highlights the unique formation of nanoplates via this green synthesis method. This system's structural complexity can lead to unique and direction-dependent properties in materials. Three axes (a, b, and c) are all of different lengths. None of the angles (α, β, γ) between the axes are 90 degrees; each angle is different. As a result, the unit cell (the smallest repeating unit in the crystal) has a very irregular shape. The lattice parameters of the phase are a = 6.13280 (10) Å, b = 7.51510 (10) Å, c = 8.58010 (10) Å, α = 98.2630 (7)°, β = 104.6220 (8)°, γ = 102.1398 (8)°.

In addition, we also observed a secondary phase that corresponded to a monoclinic crystal system, matched with reference pattern 05-001-0464. This system is defined by two axes forming 90° angles, while the third angle deviates, giving it a different symmetry. The presence of both triclinic and monoclinic phases suggests complex crystallization dynamics, likely influenced by the composition of the cork oak somatic embryo extract.

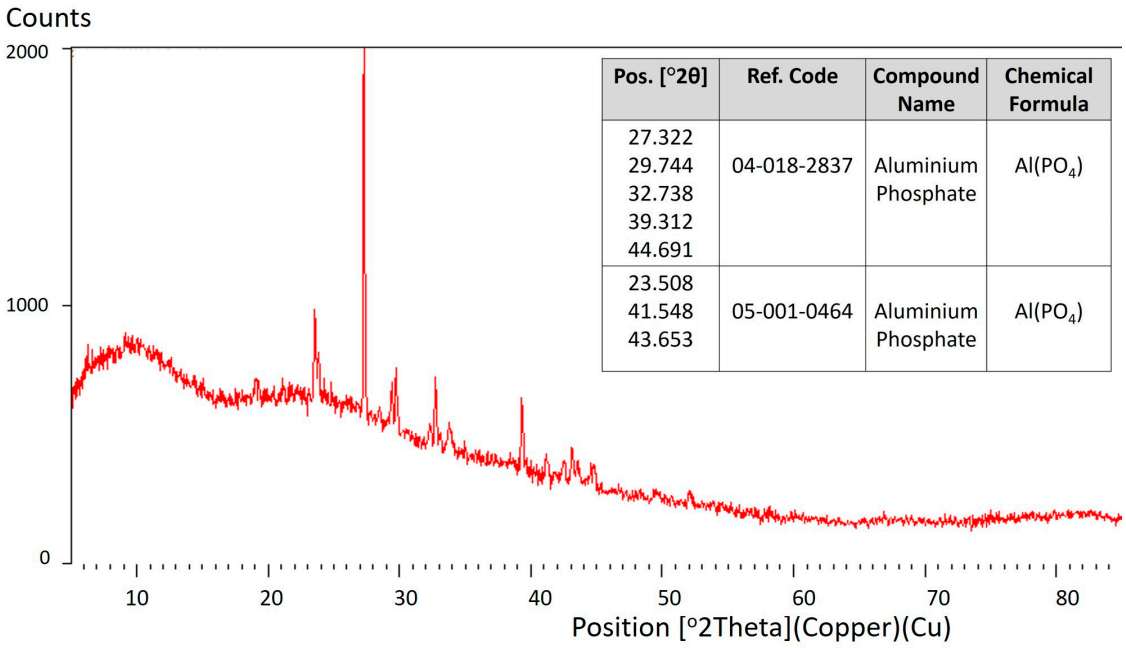

Pos. [°2θ]	Ref. Code	Compound Name	Chemical Formula
27.322 29.744 32.738 39.312 44.691	04-018-2837	Aluminium Phosphate	$Al(PO_4)$
23.508 41.548 43.653	05-001-0464	Aluminium Phosphate	$Al(PO_4)$

Figure 4. XRD profile of AlNPs obtained by reaction of *Q. suber* somatic embryos extract with $Al(NO_3)_3{\cdot}9H_2O$; in the insert, the table with the identifications. Peaks identifying the presence of aluminum phosphate have been listed.

3.5. Transmission Electron Microscopy (TEM), Scanning Electron Microscopy (SEM), and Energy-Dispersive X-ray Spectroscopy (EDX)

The transmission electron microscopy (TEM) and scanning electron microscopy (SEM) analysis provided detailed insights into the morphology and size of the aluminum nanopar-

ticles (AlNPs) synthesized. Noteworthy, the nanoparticles synthesized using cork oak somatic embryo extract exhibited a nanoplate morphology. These nanoplates were extremely thin (Figure 5A,B), transparent, and had a wide range of lateral dimensions. All types of nanoparticles were well-dispersed with minimal aggregation, indicating effective stabilization by the phytochemicals present in the plant extract.

High-resolution TEM and SEM images showed that the nanoplates had distinct edges and faces, characteristic of their crystalline nature.

The elemental composition of the nanoplates has been deduced using EDX in conjunction with SEM and TEM. The EDX analysis of the cork oak-derived nanoplates confirmed the presence of aluminum (Figure 5C,D), indicating a successful synthesis of phosphate aluminum nanoplates.

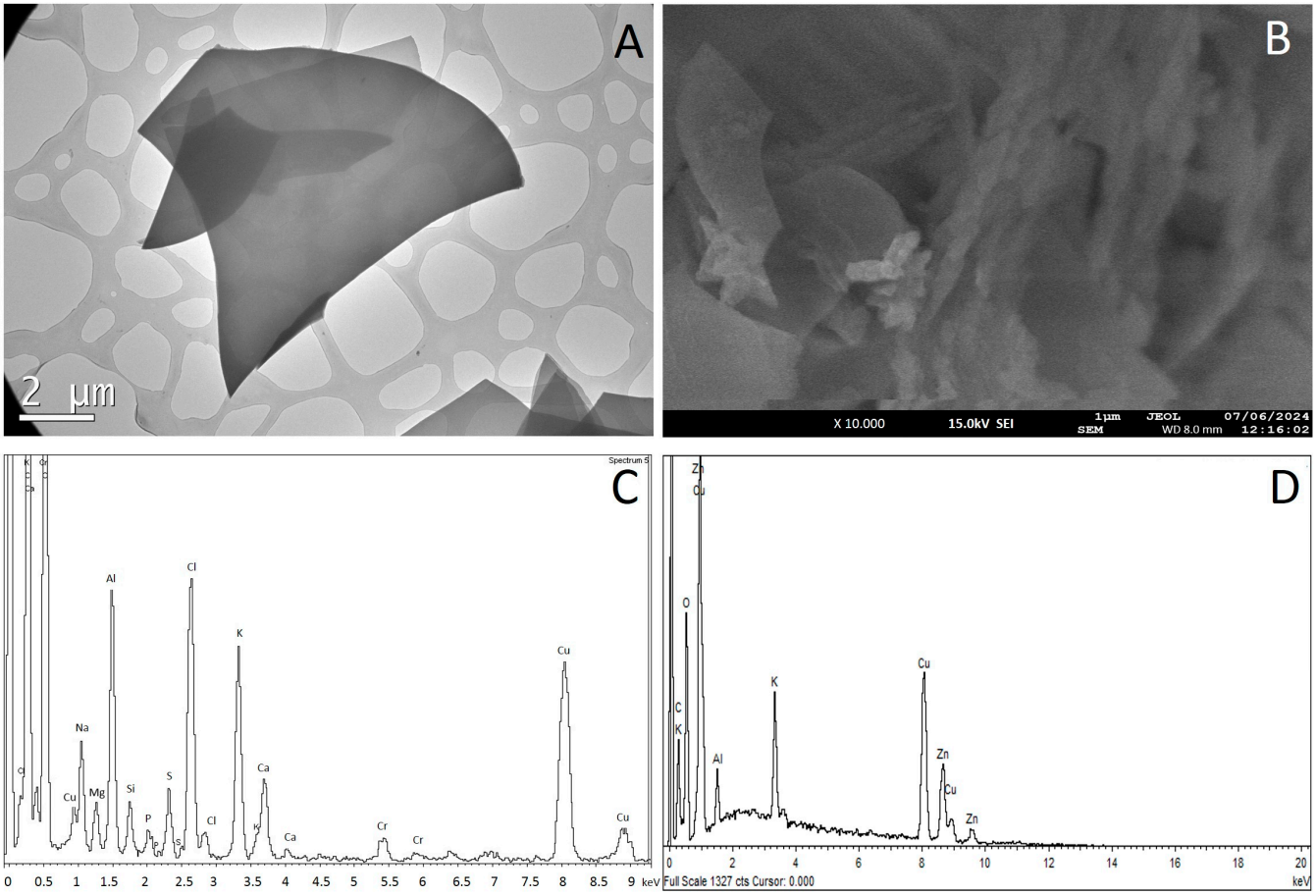

Figure 5. Transmission electron microscope (TEM) and scanning electron microscope (SEM) images and EDX spectrum showing the presence of aluminum in the aluminum phosphate nanoplates synthesized via green synthesis from aluminum nitrate nonahydrate and cork oak somatic embryo extract. (**A**) TEM image (the transparency observed is due to the extremely thin nature of the nanoplates); (**B**) SEM image; (**C**) EDX in coupling with TEM; (**D**) EDX in coupling with SEM.

3.6. Fourier-Transform Infrared Spectroscopy (FTIR)

The FTIR spectra for both the aqueous extract of cork oak somatic embryos and the aluminum nanoparticles (AlNPs) synthesized from this extract (Figure 6) reveal various characteristic peaks, indicating interactions between phytochemicals and the nanoparticles.

The prominent peak at 3343 cm^{-1} in the extract suggests the presence of hydrogen-bonded O-H groups, indicative of phenolic and polymeric compounds. The peak at 2934 cm^{-1} corresponds to the asymmetric stretching of CH_2 and CH_3 groups in alkanes. A significant peak at 1608 cm^{-1}, shifting to 1621 cm^{-1} in the AlNPs, indicates the presence of aromatic compounds and imines due to interactions with the phytochemicals.

C-H bending peaks at 1445, 1401, and 1354 cm^{-1}, suggesting CH_2 bending in alkanes and O-H bending in carboxylic acids. The peak at 1078 cm^{-1} is commonly associated with phosphate groups (PO_4^{3-}) in phytate.

The broadening and less-defined nature of the O-H stretching peak in the AlNPs spectrum at 3332 cm^{-1} indicates substantial interaction with the extract's phytochemicals. Alkyne and nitrile groups range 2328–2397 cm^{-1}; peaks in this range may denote the presence of alkynes (C≡C) or nitriles (C≡N). Peaks around 1650–1750 cm^{-1} can indicate C=O stretching vibrations of carbonyl compounds, including aldehydes, ketones, and carboxylic acids. Peaks at 1445, 1401, and 1354 cm^{-1} in the extract, shifting to 1348–1371 cm^{-1} in the AlNPs, indicate CH_2 bending in alkanes and O-H bending in carboxylic acids. Phosphate groups range 1000–1100 cm^{-1}; several peaks in this region in both spectra indicate the presence of phosphate groups (P-O). Peaks around 500 cm^{-1} in the AlNPs spectra confirm the presence of aluminum.

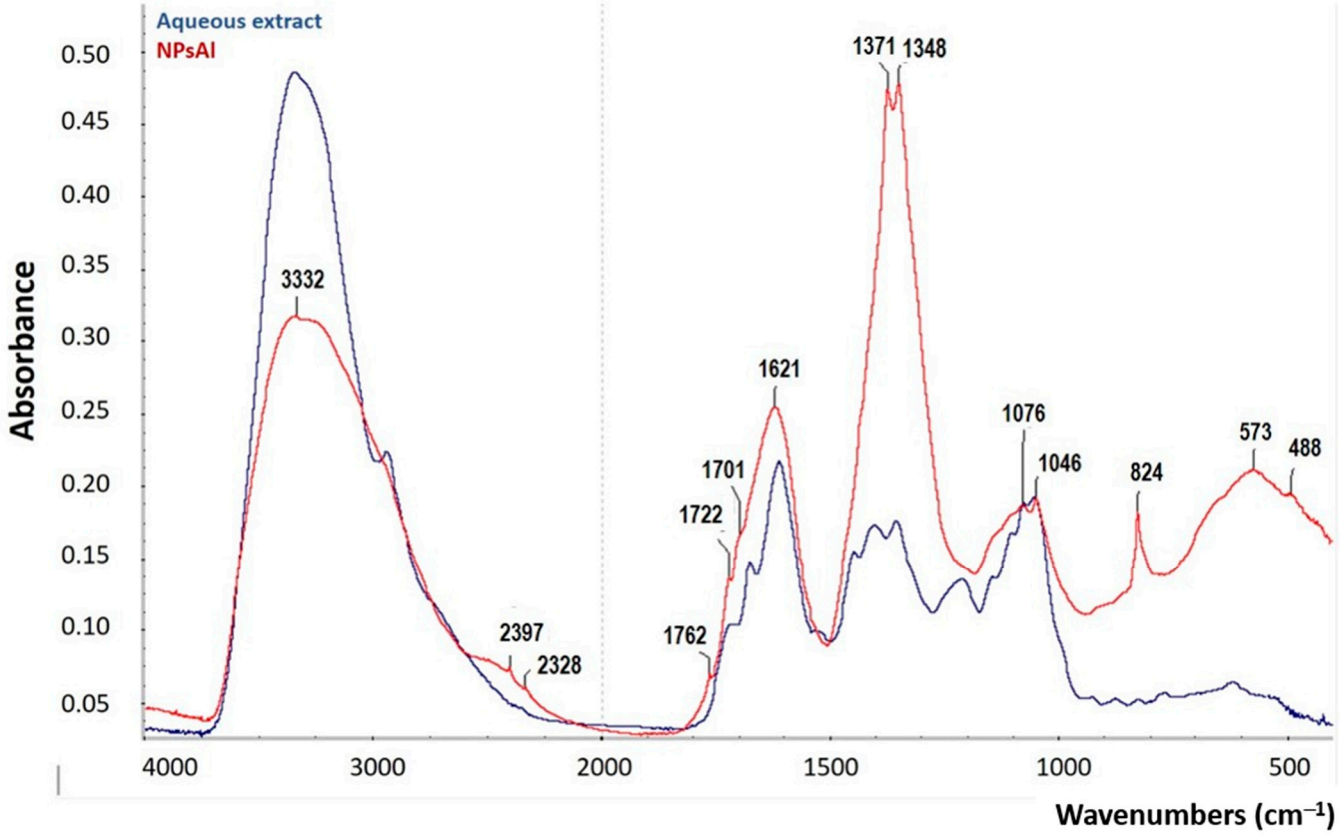

Figure 6. FTIR spectra of (blue) cork oak somatic embryos aqueous extract and (red) NPs.

4. Discussion

The synthesis of metallic nanoparticles has garnered significant interest due to its diverse applications ranging from medicine to catalysis and the electronics industry. Traditionally, nanoparticle synthesis methods employ chemical reagents and organic solvents that are harmful to the environment and costly to manage. These methods often require rigorous reaction conditions such as high temperatures and pressures to produce nanoparticles with controlled size and shape. In contrast, green methods, such as the one employed in this study, utilize plant extracts containing a variety of bioactive compounds like polyphenols, flavonoids, and terpenoids, which act as natural reducers and stabilizers of nanoparticles [16]. These biological extracts offer several advantages over traditional methods, including cost reduction, process simplicity, and the ability to produce nanoparticles with superior properties such as enhanced colloidal stability and potential biocompatible applications.

Using somatic embryos as a source of plant material can be likened to having a biofactory of secondary metabolites under controlled conditions. This approach offers distinct advantages compared to other plant extracts, as somatic embryos provide a consistent and reproducible supply of bioactive compounds. Unlike natural plant sources that can vary in chemical composition due to environmental factors, somatic embryos can be cultivated under controlled conditions, ensuring the production of metabolites in a predictable manner [25]. This controlled environment not only enhances the yield and quality of secondary metabolites but also facilitates the standardization of experimental conditions [26], making somatic embryos an ideal choice for applications requiring reliable and consistent biochemical profiles.

The characterization of this plant extract from in vitro-derived *Q. suber* somatic embryos, using UV–visible spectroscopy, revealed several significant absorbance peaks in the range from 265 to 340 nm, with specific maxima at 265, 283, 300, and 310 nm. These peaks are indicative of the presence of phenolic compounds and flavonoids (flavanones, flavanones, and isoflavones), as described by Harborne [27]. Phenolic compounds and flavonoids are well-known for their antioxidant properties and their ability to act as reducing agents in the formation of metallic nanoparticles [28]. Other plant materials similar to somatic embryos, such as plant callus cultures, have proven equally promising in the green synthesis of nanoparticles (NPs). Callus cultures are capable of producing a wide range of bioactive compounds that facilitate the reduction and stabilization of metallic NPs [29]. Nevertheless, phytates, ubiquitous in plant tissues, pose a challenge for direct spectrophotometric analysis due to their lack of specific absorption spectra, necessitating the use of indirect methods such as the molybdate blue method for detection in extracts.

Phytic acid, also known as inositol hexaphosphate or IP6, is a compound present in plants. It serves as the principal form of phosphorus storage, especially in seeds. For example, acorns of oak species exhibit significant amounts of phosphorus, although it is possible to discern species-specific distribution patterns [30]. Furthermore, phosphorus concentrations vary significantly across seed parts, notably six times lower in the pericarp and testa compared to embryos. Our study determined a substantial phosphate content of 23.6 µMol PO_4^{3-}/mg DW (equivalent to 2.24 mg/g in embryo tissue) in extracts from cork oak somatic embryos. This is much higher compared to *Quercus robur*, where phosphorus content in embryos typically ranges from 1.18 to 0.75 mg/g [31]. Probably, the species *Q. suber* and the use of somatic embryos, which lack outer coverings, may influence the high quantities of phytates in the extract.

Only water and a few minutes are necessary to completely remove the phytic acid content from plant materials [32]. The interaction of plant material with hot water causes the cell walls to rupture, allowing for soluble phytic acid to leach into the medium [33]. Given that phytic acid undergoes thermal decomposition at 150 °C for about one hour [34], we can assume that phytic acid will be present in the extract, considering the conditions we followed to produce it.

There are several properties of phytate that suggest its potential role in the green synthesis of aluminum nanoparticles. Firstly, phytate possesses multiple negative charges, which makes it an effective chelator of multivalent cations such as calcium, magnesium, and iron [35]. It forms strong complexes with mineral cations through ionic interactions with negatively charged phosphates [36]. Secondly, phytic acid serves as an important source of antioxidants [37]. For instance, Khattab et al. [38] evaluated bioactive components in canola seeds, including phytic acid, and determined its free-radical-scavenging activity using the DPPH (1,1-diphenyl-2-picrylhydrazyl) method. Their findings showed that phytic acid exhibited the highest DPPH-scavenging activity, indicating a superior antioxidant effect compared to other components like condensed tannins and chlorophyll.

Therefore, the significant role of phytate from *Q. suber* somatic embryos in the precipitation of aluminum nanoparticles in this experiment is plausible when mixed with aluminum nitrate nonahydrate. The chelation mechanism limits the free aluminum ions in solution, creating localized supersaturation conditions that promote the formation of

crystalline nanoplates rather than other morphologies. This results in the formation of a dark precipitate. The change in coloration of the aluminum nitrate solution caused by the extract of cork oak somatic embryos is characteristic of nanoparticle synthesis. The extract reacted slowly with the aluminum nitrate nonahydrate solution, producing a cloud that settled at the bottom of the container before nanoparticle precipitation occurred.

UV–VIS spectroscopy is indispensable for analyzing the optical properties of nanoparticles. The surface plasmon resonance (SPR) peak detected in UV–VIS spectra provides specific information about the optical properties of nanoparticles. The position of the SPR peak correlates directly with the size and shape of the particles, offering valuable insights into their nanoscale structure and electronic configuration [39].

The absorption peaks may be attributed to specific electronic transitions within the aluminum phosphate structure, which can be influenced by the presence of aluminum and its interaction with phosphate groups [40]. The presence of multiple peaks in the UV–VIS spectra, such as those observed at 345–360 nm and 402 nm for aluminum phosphate nanoplates, indicates their anisotropic nature [41]. Anisotropic materials exhibit varying physical properties along different axes, often due to their distinct two-dimensional shapes and crystal orientation. In the case of nanoplates, these multiple peaks correspond to different electronic excitations and surface plasmon resonance (SPR) modes, reflecting their ability to interact differently with incident light depending on their orientation. In an anisotropic material like nanoplates, the multiple SPR peaks between 345 nm and 360 nm might reflect interactions influenced by the plate's thin dimensions along certain crystallographic directions. They may be associated with plasmonic resonant modes that are sensitive to certain dimensions of the nanoplates, possibly their thickness or combinations of length and width. A prominent peak at 402 nm could also indicate specific optical resonances or plasmonic effects due to another distinct dimension of the nanoplates, such as the dominant length or width. At the nanoscale, surface effects become more pronounced. The surfaces of aluminum phosphate nanoplates may interact with light in ways distinct from bulk materials, leading to specific absorption characteristics [42].

The Full Width at Half Maximum (FWHM) provides a precise measure of the nanoparticle size distribution. A narrow FWHM indicates a more uniform size distribution, whereas a broader FWHM suggests greater variability in particle size. The narrow FWHM value of 53 nm suggests minimal variation in nanoparticle dimensions [39], which is advantageous for applications requiring precise control over optical characteristics, such as in sensors and photonic devices.

The nanoplates synthesized from cork oak have been identified as aluminum phosphate ($AlPO_4$) through XRD analysis. Previous studies characterizing aluminum phosphate nanoparticles [43–45] do not report the formation of nanoplates or utilize green synthesis methods for their formation, contrasting with our findings. Furthermore, the crystal systems identified in our nanoplates are triclinic (anorthic), a unique structure in the context of $AlPO_4$, and monoclinic. The triclinic irregular crystal structure can significantly influence the material's optical properties, potentially leading to direction-dependent behaviors such as birefringence, where the refractive index varies with the direction of light propagation [46].

$AlPO_4$ exhibits crystal structures analogous to tridymite and cristobalite found in SiO_2. However, triclinicity is not typically observed in cristobalite or tridymite phases of $AlPO_4$, which typically crystallize in tetragonal or monoclinic forms. Tridymite in $AlPO_4$ undergoes a complex transformation sequence, culminating in monoclinic and triclinic modifications at room temperature; both phases of tridymite coexist and are often intergrow in the same crystal showing unique transformation behaviors, including multiple twinning under specific conditions [47].

Thus, our discovery of monoclinic–triclinic aluminum phosphate nanoplates synthesized via green methods represents a novel route to obtain these structures, potentially offering new opportunities for applications in optoelectronics and other fields requiring directional optical properties.

Aluminum nanoparticles (AlNPs) synthesized via green synthesis from cork oak somatic embryos were also characterized using electron microscopy, TEM, and SEM. The microscopic analysis revealed aluminum nanoplates with varying sizes yet consistent structures. While not all nanoplates exhibit nanoscale dimensions uniformly across their entire area, their significant transparency suggests that nanoscale dimensions are achieved in at least one dimension in agreement with the XRD analysis. Importantly, the presence of nanoplates instead of the more commonly observed spherical shapes of aluminum nanoparticles [48,49], as evidenced in the microscopic images, underscores a unique aspect of our study. The SEM image shows an irregular and complex surface with laminar and possibly crystalline structures. The observation of large laminar formations along with smaller structures in the SEM image suggests that the sample has a hierarchical organization. The hierarchy in the structure may result from self-assembly processes, where particles spontaneously organize into ordered structures [50].

To date, the scientific literature has extensively documented the synthesis of alumina (aluminun oxide) nanoplates using various templates such as graphene oxide [51]. However, nanoplates of aluminum phosphate like ours have not been described. Our approach represents a significant advancement by demonstrating the direct synthesis of phosphate nanoplates, specifically aluminum phosphate ($AlPO_4$), without the need for a templating mold. This innovative method provides a novel pathway for obtaining nanoplate structures in aluminum materials.

The EDX analysis confirmed the presence of aluminum in the nanoplates derived from *Quercus suber* somatic embryos. In the TEM-EDX spectrum, around 2.01 keV, there is a distinct peak that corresponds to phosphorus. There are several reasons why there might be a discrepancy between the results of XRD (X-ray diffraction) and SEM-EDX (energy-dispersive X-ray spectroscopy) in detecting phosphorus in a sample of aluminum phosphate. XRD is a technique for analyzing crystalline structures that can identify compounds and phases present in the sample based on diffraction patterns. On the other hand, EDX identifies and quantifies elements present in a specific area. It is possible that XRD detects the aluminum phosphate phase in the overall sample, while EDX may not detect phosphorus if it is in a very low concentration in the analyzed region.

The green synthesis of $AlPO_4$NPs starts with the dissociation of aluminum nitrate into aluminum and nitrate ions in aqueous solution:

$$Al(NO_3)_3 \rightarrow Al^{3+} + 3NO^{3-}$$

The interaction of IP6 with cations like Al^{3+} is exclusively due to its numerous phosphate groups: these can bind to a single phosphate group, to two phosphate groups of the same molecule, or phosphate groups from different molecules of IP6 [52].

The process would be as follows:

Interaction of IP6 with aluminum: Phytic acid (IP6) contains multiple phosphate groups (PO_4^{3-}), which can coordinate with metal ions such as Al^{3+}.

Formation of chelate complexes: In a solution, Al^{3+} ions can bind to phosphate groups from different IP6 molecules to form aluminum–phosphate chelate complexes.

Cross-linking between IP6 molecules: The bonding between aluminum and phosphate groups from different IP6 molecules contributes to the formation of larger and more complex structures. This process can lead to the hierarchical organization observed in SEM images.

Self-assembly and ordered structures: These complexes and bonds facilitate self-assembly processes where IP6 molecules and Al^{3+} ions spontaneously organize into ordered structures at various scales, as observed in the hierarchical organization mentioned earlier.

FTIR analysis enabled the comparison of the plant extract used and the interactions of its phytochemicals with our $AlPO_4$NPs. As observed in the results, the FTIR absorption spectrum of the *Quercus suber* L. extract shows several peaks similar to those observed in the FTIR spectrum of the $AlPO_4$NPs.

The hydroxyl groups (OH) in phytic acid can exhibit bending vibrations in the FTIR spectrum. The bending vibrations of O-H typically appear in the range of 3200 to 3600 cm^{-1}. The first peak in the extract appears at 3343 cm^{-1}, indicating hydrogen bonds (O-H). The peak at 1608 cm^{-1} in the extract shifts to 1624 cm^{-1} in the $AlPO_4$NPs, indicating possible interactions with aromatic compounds. In phytic acid, the CH_2 groups are present in the cyclohexane ring that is part of the structure of IP6. The bending vibrations of the CH_2 groups observed at 1445, 1401, and 1354 cm^{-1} in the extract shift to 1348–1398 cm^{-1} in the $AlPO_4$NPs. The peak at 1076 cm^{-1} in the extract is attributed to the phosphate groups of phytate [53]. Additionally, several peaks at 1000–1100 cm^{-1} in both spectra indicate the presence of phosphate groups (P-O), as described in phytates [54], corresponding mainly to the $\nu as(PO_4)$ and $\nu s(PO_4)$ stretching vibrations [55]. The peak at 824 cm^{-1} and one broad band with a shoulder around 1300–900 cm^{-1} is characteristic of the trivalent compound Al-IP6 [56]. Finally, the maximum of the $\delta as(PO_4)$ band shifts at 488 cm^{-1} for Al-IP6.

In conclusion, the green synthesis of aluminum phosphate ($AlPO_4$) nanoplates using extracts from *Quercus suber* somatic embryos represents a significant advancement in nanomaterials research. This study harnesses the unique properties of somatic embryos, providing a consistent and reproducible source of bioactive compounds such as phytic acid (IP6), which act in nanoparticle formation. The synthesized nanoplates exhibit distinct optical properties evidenced by UV–VIS spectroscopy, showcasing multiple absorption peaks indicative of their anisotropic structure inferred from XRD analysis. Characterization through electron microscopy and FTIR spectroscopy further confirms their nanoscale dimensions and chemical composition. The hierarchical organization observed in SEM images suggests self-assembly processes, highlighting the innovative potential of this green synthesis approach. This novel pathway not only expands our understanding of aluminum phosphate nanoplate formation but also opens doors for future applications in fields requiring directional optical properties and advanced nanomaterials.

Aluminum phosphates have a broad range of applications, as highlighted by Goj et al. [57]. The unique properties of aluminum phosphate nanoplates are crucial in determining their potential across various fields. For example, studies have shown that hexagonal and square planar morphologies of zinc aluminum phosphate nanoplates enhance catalytic activity, particularly in biofuel production [58]. Additionally, the nanoporous structure of aluminum phosphates has shown promise as electrode materials for energy storage, offering superior capacitance and retention [59]. The self-assembly of these nanoplates into chain-like architectures has also been found to improve charge transport and active site availability in oxygen evolution reaction (OER) catalysis [60]. Their potential as a vaccine adjuvant has been explored as well, with aluminum phosphate nanoparticles stabilized by amino acids demonstrating biocompatibility without affecting antigen-specific antibody production [61]. Furthermore, similar nanoplates have been employed in drug-delivery systems, offering enhanced protein loading and controlled release [62]. Aluminum phosphate nanostructures also show promise as flame-retardant materials, owing to their stable 3D core-shell structures [63]. Recent research highlights the electrorheological behavior of anhydrous aluminum orthophosphate particles with tridymite-like structures, showcasing their potential in advanced rheological applications [64]. Additionally, the strong interaction of aluminum (III) with biomolecular phosphates such as ATP suggests significant roles in biological processes like enzymatic reactions and signal transduction [65]. These findings underscore the diverse potential applications of aluminum phosphate nanoplates, demonstrating that their unique properties not only enhance performance in established areas but may also lead to novel applications in advanced materials, environmental remediation, and biomedicine. Future research will continue to explore these possibilities, building on the foundational synthesis and characterization presented in this study.

5. Conclusions

The green synthesis of aluminum phosphate ($AlPO_4$) nanoplates using extracts from *Quercus suber* somatic embryos represents a notable advancement in sustainable nano-

material production. This study demonstrates that plant-derived bioactive compounds, particularly phytic acid, can effectively promote the formation of nanoplates under environmentally benign conditions. Characterization techniques, including UV–Vis spectroscopy, XRD, TEM, and SEM, revealed distinct optical and structural properties. Importantly, both monoclinic and triclinic crystal phases of tridymite were identified, highlighting the complexity and uniqueness of the synthesized nanoplates. These dual phases may offer novel opportunities for applications requiring specific optical and structural characteristics. This study underscores the potential of plant-based materials for the sustainable production of advanced nanomaterials and opens avenues for future research on the scalability and practical applications of these nanoplates.

Author Contributions: Conceptualization, B.P. and A.G.-G.; Methodology, B.P. and A.G.-G.; Validation, B.P. and A.G.-G.; Formal analysis, B.P. and A.G.-G.; Investigation, B.P. and A.G.-G.; Resources, B.P. and A.G.-G.; Data curation, B.P. and A.G.-G.; Writing—original draft, B.P. and A.G.-G.; Writing—review & editing, A.G.-G.; Visualization, B.P. All authors have read and agreed to the published version of the manuscript.

Funding: This research received no external funding.

Institutional Review Board Statement: Not applicable.

Informed Consent Statement: Not applicable.

Data Availability Statement: Data is contained within the article.

Conflicts of Interest: The authors declare no conflicts of interest.

References

1. Ghorbani, H.R. A review of methods for synthesis of Al nanoparticles. *Orient. J. Chem.* **2014**, *30*, 1941–1949. [CrossRef]
2. Iqbal, I.; Sharma, S.; Pathania, A.R. An insight into application and harmful effects of aluminum, aluminum complexes and aluminum nano-particles. *Mater. Today Proc.* **2022**, *62*, 4365–4369. [CrossRef]
3. Elaiyappillai, E.; Arumugam, G.; Johnson, P.M.; Kogularasu, S.; Rajendran, R. Sonochemical assisted leaching of aluminum oxide nanoparticles from domestic aluminum wastes as non-toxic electrode material for energy storage application. *J. Electrochem. Soc.* **2020**, *167*, 110541. [CrossRef]
4. AbdulKarim-Talaq, M.; Hassan, K.T.; Hameed, D.A. Improvement of thermal conductivity of novel asymmetric dimeric coumarin liquid crystal by doping with boron nitride and aluminum oxide nanoparticles. *Mater. Chem. Phys.* **2023**, *297*, 127367. [CrossRef]
5. Hassanpour, P.; Panahi, Y.; Ebrahimi-Kalan, A.; Akbarzadeh, A.; Davaran, S.; Nasibova, A.N.; Kavetskyy, T. Biomedical applications of aluminum oxide nanoparticles. *Micro Nano Lett.* **2018**, *13*, 1227–1231. [CrossRef]
6. Mukherjee, A.; Sadiq, I.M.; Prathna, T.C.; Chandrasekaran, N. Antimicrobial activity of aluminum oxide nanoparticles for potential clinical applications. *Sci. Against Microb. Pathog. Commun. Curr. Res. Technol. Adv.* **2011**, *1*, 245–251.
7. Maharjan, A.; Gautam, R.; Lee, G.; Kim, D.; Lee, D.; Acharya, M.; Kim, H.; Heo, Y.; Kim, C. Assessment of skin sensitization potential of zinc oxide, aluminum oxide, manganese oxide, and copper oxide nanoparticles through the local lymph node assay: 5-bromo-deoxyuridine flow cytometry method. *J. Toxicol. Environ. Health Part A* **2024**, 1–11. [CrossRef] [PubMed]
8. Honda, J.; Sugawa, K.; Tahara, H.; Danno, M.; Suzuki, A.; Kurumi, S.; Kimura, T.; Kosuge, Y.; Ikake, H.; Hashimoto, T.; et al. Photothermal Therapeutic Nanomaterials Composed of Plasmonic Aluminum Nanostructures for Effective Killing of Cells. *ACS Appl. Nano Mater.* **2024**, *7*, 2889–2902. [CrossRef]
9. González-Gómez, M.A.; Belderbos, S.; Yañez-Vilar, S.; Piñeiro, Y.; Cleeren, F.; Bormans, G.; Deroose, C.M.; Gsell, W.; Himmelreich, U.; Rivas, J. Development of superparamagnetic nanoparticles coated with polyacrylic acid and aluminum hydroxide as an efficient contrast agent for multimodal imaging. *Nanomaterials* **2019**, *9*, 1626. [CrossRef]
10. Isitman, N.A.; Dogan, M.; Bayramli, E.; Kaynak, C. The role of nanoparticle geometry in flame retardancy of polylactide nanocomposites containing aluminum phosphinate. *Polym. Degrad. Stab.* **2012**, *97*, 1285–1296. [CrossRef]
11. Cai, G.; Wu, J.; Guo, J.; Wan, Y.; Zhou, Q.; Zhang, P.; Yu, X.; Wang, M. A novel inorganic aluminum phosphate-based flame retardant and thermal insulation coating and performance analysis. *Materials* **2023**, *16*, 4498. [CrossRef] [PubMed]
12. Xu, X.; Zhang, J.; Jiang, P.; Liu, D.; Jia, X.; Wang, X.; Zhou, F. Direct ink writing of aluminum-phosphate-bonded Al2O3 ceramic with ultra-low dimensional shrinkage. *Ceram. Int.* **2022**, *48*, 864–871. [CrossRef]
13. Gou, Y.; Xie, Y.; Shen, S.; Xing, H.; Jin, P.; Li, H.; Chao, X.; Hu, D. Enhancement of aluminum phosphate adhesion performance by nano-clay for terracotta figurine restoration. *Int. J. Adhes. Adhes.* **2024**, *132*, 103685. [CrossRef]
14. Kumar, N.; Biswas, K. Cryomilling: An environment friendly approach of preparation large quantity ultra refined pure aluminum nanoparticles. *J. Mater. Res. Technol.* **2019**, *8*, 63–74. [CrossRef]

15. Tran, G.T.; Nguyen, N.T.H.; Nguyen, N.T.T.; Nguyen, T.T.T.; Nguyen, D.T.C.; Tran, T.V. Plant extract-mediated synthesis of aluminum oxide nanoparticles for water treatment and biomedical applications: A review. *Environ. Chem. Lett.* **2023**, *21*, 2417–2439. [CrossRef]
16. Al-Zahrani, S.; Astudillo-Calderón, S.; Pintos, B.; Pérez-Urria, E.; Manzanera, J.A.; Martín, L.; Gomez-Garay, A. Role of synthetic plant extracts on the production of silver-derived nanoparticles. *Plants* **2021**, *10*, 1671. [CrossRef]
17. Kumar, V.; Sinha, A.K.; Makkar, H.P.; Becker, K. Dietary roles of phytate and phytase in human nutrition: A review. *Food Chem.* **2010**, *120*, 945–959. [CrossRef]
18. Ravindran, V.; Ravindran, G.; Sivalogan, S. Total and phytate phosphorus contents of various foods and feedstuffs of plant origin. *Food Chem.* **1994**, *50*, 133–136. [CrossRef]
19. Reinmuth, M.; Pramanik, S.; Douglas, J.T.; Day, V.W.; Bowman-James, K. Structural impact of chelation on phytate, a highly phosphorylated biomolecule. *Eur. J. Inorg. Chem.* **2019**, *2019*, 1870–1874. [CrossRef]
20. Kumar, A.; Dash, G.K.; Sahoo, S.K.; Lal, M.K.; Sahoo, U.; Sah, R.P.; Ngangkham, U.; Kumar, S.; Baig, M.J.; Sharma, S.; et al. Phytic acid: A reservoir of phosphorus in seeds plays a dynamic role in plant and animal metabolism. *Phytochem. Rev.* **2023**, *22*, 1281–1304. [CrossRef]
21. Reid, D.A.; Lott, J.N.; Attree, S.M.; Fowke, L.C. Mineral nutrition in white spruce (*Picea glauca* [Moench] Voss) seeds and somatic embryos. I. phosphorus, phytic acid, potassium, magnesium, calcium, iron and zinc. *Plant Sci.* **1999**, *141*, 11–18. [CrossRef]
22. Gomez-Garay, A.; Manzanera, J.A.; Pintos-Lopez, B. Embryogenesis in Oak species. *A review. For. Syst.* **2014**, *23*, 191–198.
23. Adewale, O.B.; Egbeyemi, K.A.; Onwuelu, J.O.; Potts-Johnson, S.S.; Anadozie, S.O.; Fadaka, A.O.; Osukoya, O.A.; Aluko, B.T.; Johnson, J.; Obafemi, T.O.; et al. Biological synthesis of gold and silver nanoparticles using leaf extracts of Crassocephalum rubens and their comparative *in vitro* antioxidant activities. *Heliyon* **2020**, *6*, e05501. [CrossRef] [PubMed]
24. Callejas, F.R. *Tablas de Espectroscopía Infrarroja*; Departamento de Física y Química, UNAM (Universidad Nacional Autónoma de México): Mexico City, Mexico, 2000.
25. Gomez-Garay, A.; Lopez, J.A.; Camafeita, E.; Bueno, M.A.; Pintos, B. Proteomic perspective of *Quercus suber* somatic embryogenesis. *J. Proteom.* **2013**, *93*, 314–325. [CrossRef] [PubMed]
26. Murthy, H.N.; Joseph, K.S.; Hahn, J.E.; Lee, H.S.; Paek, K.Y.; Park, S.Y. Suspension culture of somatic embryos for the production of high-value secondary metabolites. *Physiol. Mol. Biol. Plants* **2023**, *29*, 1153–1177. [CrossRef]
27. Harborne, A.J. *Phytochemical Methods a Guide to Modern Techniques of Plant Analysis*; Springer Science & Business Media: Berlin/Heidelberg, Germany, 1998.
28. Amini, S.M.; Akbari, A. Metal nanoparticles synthesis through natural phenolic acids. *IET Nanobiotechnol.* **2019**, *13*, 771–777. [CrossRef]
29. Nabikhan, A.; Kandasamy, K.; Raj, A.; Alikunhi, N.M. Synthesis of antimicrobial silver nanoparticles by callus and leaf extracts from saltmarsh plant, *Sesuvium portulacastrum* L. *Colloids Surf. B Biointerfaces* **2010**, *79*, 488–493. [CrossRef] [PubMed]
30. Castro, L.M.G.; Ribeiro, T.B.; Machado, M.; Alexandre, E.M.C.; Saraiva, J.A.; Pintado, M. Unraveling the Effect of Dehulling Methods on the Nutritional Composition of Acorn *Quercus* spp. *J. Food Compos. Anal.* **2022**, *106*, 104354. [CrossRef]
31. Nikolic, N.; Orlovic, S.; Krstic, B.; Kevrešan, Ž. Variability of acorn nutrient concentrations in pedunculate oak (*Quercus robur* L.) genotypes. *J. For. Sci.* **2006**, *52*, 51–60. [CrossRef]
32. Graf, E. Applications of phytic acid. *J. Am. Oil Chem. Soc.* **1983**, *60*, 1861–1867. [CrossRef]
33. Yadav, S.K.; Sehgal, S. Effect of domestic processing and cooking on selected antinutrient contents of some green leafy vegetables. *Plant Foods Hum. Nutr.* **2003**, *58*, 1–11. [CrossRef]
34. Daneluti, A.L.M.; Velasco, M.V.R.; Baby, A.R.; Matos, J.D.R. Thermal behavior and free-radical-scavenging activity of phytic acid alone and incorporated in cosmetic emulsions. *Cosmetics* **2015**, *2*, 248–258. [CrossRef]
35. Luttrell, B.M. The biological relevance of the binding of calcium ions by inositol phosphates. *J. Biol. Chem.* **1993**, *268*, 1521–1524. [CrossRef] [PubMed]
36. Jung, N.C.; Tamai, Y. Polyphosphate (phytate) formation in *Quercus acutissima-Scleroderma verrucosum* ectomycorrhizae supplied with phosphate. *J. Plant Interact.* **2013**, *8*, 291–303. [CrossRef]
37. Upadhyay, J.; Tiwari, N.; Durgapal, S.; Jantwal, A.; Kumar, A. Phytic acid: As a natural antioxidant. In *Antioxidants Effects in Health*; Elsevier: Amsterdam, The Netherlands, 2022; pp. 437–450.
38. Khattab, R.; Goldberg, E.; Lin, L.; Thiyam, U. Quantitative analysis and free-radical-scavenging activity of chlorophyll, phytic acid, and condensed tannins in canola. *Food Chem.* **2010**, *122*, 1266–1272. [CrossRef]
39. Jimenez, B.C.; Sarmanho, G.; Murphy, K.E.; Bustos, A.R.M.; Baudrit, J.R.V. NanoUV-VIS: An interactive visualization tool for monitoring the evolution of optical properties of nanoparticles throughout synthesis reactions. *J. Res. Natl. Inst. Stand. Technol.* **2017**, *122*, 1.
40. Qi, Y.; Qi, H.; Li, J.; Lu, C. Synthesis, microstructures and UV–vis absorption properties of β-Ni (OH) 2 nanoplates and NiO nanostructures. *J. Cryst. Growth* **2008**, *310*, 4221–4225. [CrossRef]
41. Liu, Y.; Liu, K.; Yang, M.; Han, Y.; Zhang, Q.; Conde, J.; Yang, Y.; Alfranca, G.; Wang, Y.; Ma, L.; et al. Gastric parietal cell and intestinal goblet cell secretion: A novel cell-mediated in vivo metal nanoparticle metabolic pathway enhanced with diarrhea via Chinese herbs. *Nanoscale Res. Lett.* **2019**, *14*, 1–13. [CrossRef]
42. Martin, J.; Plain, J. Fabrication of aluminum nanostructures for plasmonics. *J. Phys. D Appl. Phys.* **2014**, *48*, 184002. [CrossRef]

43. Mekky, W.; Nicholson, P.S. Nano-aluminum-phosphate via a polymerized organic-inorganic complex route. *J. Mater. Process. Technol.* **2007**, *190*, 393–396. [CrossRef]
44. Devamani, R.H.P.; Alagar, M. Synthesis and characterization of aluminum phosphate nanoparticles. *Int. J. Appl. Sci. Eng. Res.* **2012**, *1*, 769–775. [CrossRef]
45. Peplinski, B.; Adamczyk, B.; Formanek, P.; Meyer, C.; Krüger, O.; Scharf, H.; Reinsch, S.; Ostermann, M.; Nofz, M.; Jäger, C.; et al. Nanocrystalline and stacking-disordered β-cristobalite $AlPO_4$ chemically stabilized at room temperature: Synthesis, physical characterization, and X-ray powder diffraction data. *Powder Diffr.* **2017**, *32*, S193–S200. [CrossRef]
46. Chattopadhyay, A. Wave reflection in triclinic crystalline medium. *Arch. Appl. Mech.* **2006**, *76*, 65–74. [CrossRef]
47. Graetsch, H. Two forms of aluminum phosphate tridymite from X-ray powder data. *Acta Crystallogr. Sect. C Cryst. Struct. Commun.* **2000**, *56*, 401–403. [CrossRef] [PubMed]
48. Chang, H.; Chang, Y.C. Fabrication of Al_2O_3 nanofluid by a plasma arc nanoparticles synthesis system. *J. Mater. Process. Technol.* **2008**, *207*, 193–199. [CrossRef]
49. Nayak, S.S.; Wadhawa, G.C.; Shivankar, V.S.; Inamadar, R.F.; Sonawale, C. Green synthesis of nanostructured aluminum: Antibacterial activity and dye degradation. *Eur. J. Mol. Clin. Med* **2020**, *7*, 2640–2654.
50. Rajapaksha, R.D.A.A. Self-assembling smart materials for biomaterials applications. In *Polymer Nanocomposite-Based Smart Materials*; Woodhead Publishing: Sawston, UK, 2020; pp. 121–147.
51. Mustafa, T.; Aslam, M.M.A.; Ruiz, K.H.; Javed, M.; Gao, J.; Sharif, M.H.; Khan, S. Fabrication of mechanically strong Al2O3 nanoplates derived monolithic ceramic. *Ceram. Int.* **2023**, *49*, 40478–40485. [CrossRef]
52. Martínez Domínguez, B.; Ibáñez Gómez, M.; Rincón León, F. Acido fítico: Aspectos nutricionales e implicaciones analíticas. *Arch. Latinoam. Nutr.* **2002**, *52*, 219–231.
53. Quiñone, D.; Veiga, N.; Savastano, M.; Torres, J.; Bianchi, A.; Kremer, C.; Bazzicalupi, C. Supramolecular interaction of inositol phosphates with Cu (ii): Comparative study of Ins P 6–Ins P 3. *CrystEngComm* **2022**, *24*, 2126–2137. [CrossRef]
54. Ishiguro, T.; Ono, T.; Nakasato, K.; Tsukamoto, C.; Shimada, S. Rapid measurement of phytate in raw soymilk by mid-infrared spectroscopy. *Biosci. Biotechnol. Biochem.* **2003**, *67*, 752–757. [CrossRef]
55. Zając, A.; Dymińska, L.; Lorenc, J.; Kaczmarek, S.M.; Leniec, G.; Ptak, M.; Hanuza, J. Spectroscopic properties and molecular structure of copper phytate complexes: IR, Raman, UV–Vis, EPR studies and DFT calculations. *JBIC J. Biol. Inorg. Chem.* **2019**, *24*, 11–20. [CrossRef] [PubMed]
56. Sakai, H.; Ikemoto, Y.; Kinoshita, T.; Moriwaki, T.; Yoshida, K.T. Fourier-transform spectra of metal salts of phytic acid in the mid-to far-infrared spectral range. *Vib. Spectrosc.* **2017**, *92*, 215–219. [CrossRef]
57. Goj, P.; Handke, B.; Stoch, P. Vibrational characteristics of aluminum–phosphate compounds by an experimental and theoretical approach. *Sci. Rep.* **2022**, *12*, 17495. [CrossRef] [PubMed]
58. Viswanadham, N.; Saxena, S.K.; Sreenivasulu, P. Facile synthesis of bio-fuel from glycerol over zinc aluminium phosphate nanoplates. *Sustain. Energy Fuels* **2017**, *1*, 1018–1022. [CrossRef]
59. Pramanik, M.; Salunkhe, R.R.; Imura, M.; Yamauchi, Y. Phosphonate-derived nanoporous metal phosphates and their superior energy storage application. *ACS Appl. Mater. Interfaces* **2016**, *8*, 9790–9797. [CrossRef]
60. Septiani, N.L.W.; Kaneti, Y.V.; Fathoni, K.B.; Kani, K.; Allah, A.E.; Yuliarto, B.; Nugraha; Dipojono, H.K.; Alothman, Z.A.; Golberg, D.; et al. Self-assembly of two-dimensional bimetallic nickel–cobalt phosphate nanoplates into one-dimensional porous chainlike architecture for efficient oxygen evolution reaction. *Chem. Mater.* **2020**, *32*, 7005–7018. [CrossRef]
61. Vrieling, H.; Ballestas, M.; Hamzink, M.; Willems, G.; Soema, P.; Jiskoot, W.; Kersten, G.; Metz, B. Stabilised aluminium phosphate nanoparticles used as vaccine adjuvant. *Colloids Surf. B Biointerfaces* **2019**, *181*, 648–656. [CrossRef]
62. Reardon, P.; Huang, J.; Tang, J. Morphology Controlled Porous Calcium Phosphate Nanoplates and Nanorods with Enhanced Protein Loading and Release Functionality. *Adv. Healthc. Mater.* **2013**, *2*, 682–686. [CrossRef]
63. Palacios, E.; Leret, P.; Mata, M.; Fernández, J.; Aza, A.; Rodríguez, M.; Rubio-Marcos, F. Self-Forming 3D Core-Shell Ceramic Nanostructures for Halogen-Free Flame Retardant Materials. *ACS Appl. Mater. Interfaces* **2016**, *8*, 9462–9471. [CrossRef]
64. Eshchenko, L.S.; Korobko, E.V.; Paniatouski, A.V. Preparation and electrorheological properties of anhydrous aluminum orthophosphate. *Inorg. Mater.* **2023**, *59*, 75–80. [CrossRef]
65. Luque, N.B.; Mujika, J.I.; Rezabal, E.; Ugalde, J.M.; Lopez, X. Mapping the affinity of aluminum (III) for biophosphates: Interaction mode and binding affinity in 1: 1 complexes. *Phys. Chem. Chem. Phys.* **2014**, *16*, 20107–20119. [CrossRef] [PubMed]